Detection and Quantification of Live, Apoptotic, and Necrotic Human Peripheral Lymphocytes by Single-Laser Flow Cytometry

TERI J. LIEGLER,[1]* WILLIAM HYUN,[1,2] T. S. BENEDICT YEN,[3] AND DANIEL P. STITES[1]

Laboratory for Cell Analysis, Division of Molecular Cytometry,[2] Department of Laboratory Medicine,[1] and Department of Pathology, Veterans Affairs Medical Center,[3] University of California, San Francisco, California

Regulation of peripheral lymphocyte number involves a poorly understood balance between cell renewal and loss. Disrupting this balance leads to a large number of disease states. Methods which allow qualitative and quantitative measurements of cell viability are increasingly valuable to studies directed at revealing the mechanisms underlying apoptotic and necrotic cell death. Here, we have characterized a method using single-laser flow cytometry that differentiates and quantifies the relative number of live, apoptotic, and late-stage apoptotic and necrotic peripheral lymphocytes. Following in vitro gamma irradiation and staining with acridine orange in combination with ethidium bromide, three distinct populations were seen by bivariate analysis of green versus red fluorescence. The identity of each distinct fluorescent population (whether live, apoptotic, or necrotic) was determined by sorting and examination of cellular morphology by electron microscopy. This flow cytometric method is directly compared with the techniques of trypan blue exclusion and DNA fragmentation to quantify cell death following exposure to various doses of in vitro gamma irradiation and postirradiation incubation times. We extend our findings to illustrate the utility of this method beyond analyzing radiation-induced apoptotic peripheral blood mononuclear cells (PBMC); similar fluorescent patterns are shown for radiation- and corticosteroid-treated murine thymocytes, activated human PBMC, and PBMC from human immunodeficiency virus-infected individuals. Our results demonstrate that dual-parameter flow cytometric analysis of acridine orange-ethidium bromide-stained lymphocytes is overall a superior method with increased sensitivity, greater accuracy, and decreased subjectivity in comparison with the other methods tested. By using standard laser and filter settings commonly available to flow cytometric laboratories, this method allows rapid measurement of a large number of cells from a heterogeneous sample.

Multicellular eukaryotes regulate net cell number during normal physiological growth and function by a combination of cell proliferation and death. Initiation and completion of physiological cell death, a process which is termed apoptosis (28), are intrinsic to individual cells and are controlled genetically. This process is in contrast to accidental cell death, or necrosis, which results from severe environmental perturbations. Evidence for apoptotic cell death is seen in embryonic development, normal tissue turnover, selection against autoreactive immune cells, and hormone-induced atrophy of target tissues and organs (7, 9, 47). There is great interest in understanding the molecular events involved in the induction and processes of apoptosis, in that such events may be key to regulation of normal cell growth (18, 26, 44, 48). Not surprisingly, aberrant induction of apoptosis has been implicated in many disease processes, such as cancer, autoimmunity, central nervous system degeneration, and AIDS (4). It is conceivable that effective diagnostic and therapeutic strategies may be designed on the basis of the genetic and biochemical events involved in apoptosis. Therefore, methods to accurately characterize and quantify apoptotic cells have become increasingly important in further understanding apoptosis in normal and disease processes.

There are a variety of strategies possible in developing methodologies that differentiate live from apoptotic and necrotic cells. The more widely used methods, which are based on characteristic biochemical and morphologic changes in apoptotic versus necrotic cells, include transmission and light microscopy, analysis of DNA fragmentation using gel electrophoresis or DNA quantification assays (17, 39), in situ DNA-labeling techniques (19, 20), and analysis of nuclear chromatin by fluorescent DNA-binding dyes and flow cytometry (11, 16, 24, 27–30, 33–35, 37–42, 49). Electron microscopy is considered the "gold standard" by which characteristic apoptotic features such as nuclear and chromatin condensation and the presence of apoptotic bodies and unaltered cytoplasmic organelles are clearly distinguishable. However, this method has an inherent degree of subjectivity and is inappropriate for screening a large number of cells. Similarly, less-time-consuming methods such as visualization of cells stained with supravital dyes, DNA-binding stains, or fluorescent dyes may yield inaccurate results (36). Oligomeric DNA fragmentation is not always associated with apoptosis alone and can be used to quantify the relative number of apoptotic cells only if complete oligomeric fragmentation of DNA into low-molecular-weight species occurs. This property cannot be assumed in all cells under all induction conditions (2, 6, 10, 36).

In this report, we describe a method to accurately and rapidly quantify apoptotic lymphocytes from peripheral blood mononuclear cells (PBMC). By using single-laser multiparameter flow cytometry on unfixed cells, live lymphocytes may be distinguished from early- and late-stage apoptotic and necrotic cells on a single-cell basis when they are stained with acridine orange (AO) and ethidium bromide (EB). AO-EB staining has been reported in studies of apoptosis in human immunodeficiency virus (HIV) infections (21, 22). However, the claims that

* Corresponding author. Present address: Gladstone Institute of Virology and Immunology, P.O. Box 419100, San Francisco, CA 94110. Phone: (415) 695-3806. Fax: (415) 826-1514.

the AO^{low} lymphocyte population represent apoptotic cells are not supported by direct experimental evidence. Here, we characterize the distinct AO-EB staining populations of radiation-induced apoptotic PBMC by sorting and ultrastructural morphology. We have compared the results of this flow cytometric-based assay with those from other widely used assays for apoptosis, such as vital dye exclusion and DNA fragmentation, using PBMC undergoing radiation-induced apoptosis. Our results are of interest to many types of studies in which accurate quantification of apoptosis is necessary on a single-cell basis with limited and heterogeneous samples.

MATERIALS AND METHODS

Cell preparation and culturing. Human PBMC were isolated from heparinized whole blood by density gradient centrifugation (Histopaque [ρ = 1.077]; Sigma, St. Louis, Mo.). Cells were irradiated by using a ^{137}Cs source (dose rate = 350 rads/min) at a concentration of 10^7 cells per ml in culture medium (RPMI 1640 supplemented with 10% fetal bovine serum, 10 U of penicillin G per ml, 100 μg of streptomycin per ml, and 0.3 g of L-glutamine per liter [GIBCO]) and were incubated at 2×10^6 cells per ml for the appropriate length of time at 37°C in 5% CO_2–95% air. Cell viability was determined using vital dye exclusion (0.4% trypan blue), AO-EB staining and flow cytometry, and visualization of DNA fragmentation by agarose gel electrophoresis.

PBMC were activated in vitro by addition of the CD4 T-cell-specific superantigen *Staphylococcus aureus* enterotoxin B (SEB; Sigma) at 1 μg/ml. During this culture period, lymphocyte blast formation and expression of various cell surface activation markers were observed, along with a decrease in overall viability (by trypan blue exclusion) compared with resting lymphocyte cultures from the same donor.

Thymocytes were prepared from 2- to 6-week-old mice. Thymuses were removed and made into a single-cell suspension in phosphate-buffered saline (PBS) supplemented with 0.5% bovine serum albumin. Cells were plated at 2×10^6 cells per ml in culture medium following irradiation at 500 rads (5 Gy) or treatment with 10^{-7} M dexamethasone (Sigma). After a 24-h incubation at 37°C, the thymocytes were harvested for DNA extraction (39) or AO-EB staining.

DNA extraction. Whole cellular DNA was isolated from human PBMC. Cells were pelleted and lysed with 1% sodium dodecyl sulfate in TE (10 mM Tris [pH 8.0], 0.5 mM EDTA), and digested by proteinase K (100 μg/ml; Boehringer Mannheim Biochemicals, Indianapolis, Ind.) for 2 to 4 h at 56°C. Samples were extracted with phenol and chloroform, and the DNA was precipitated with a 1/10 volume of 3 M sodium acetate and an equal volume of ethanol. DNA was pelleted at 15,000 × g and resuspended in TE and 10 μg of DNase-free RNase (Boehringer Mannheim Biochemicals) per ml for 30 min at 37°C. Low-molecular-weight DNA from irradiated mouse thymus was prepared as described elsewhere (39). DNA samples were fractionated on a 1.5% agarose gel in Tris-acetate buffer (0.04 M Tris acetate, 2 mM EDTA) by electrophoresis at 25 V for 15 h. The DNA was stained with EB (0.5 μg/ml), destained, and visualized with 254-nm-wavelength UV light.

Electron microscopy. Cells were fixed in 2% glutaraldehyde in PBS, postfixed in osmium tetroxide, dehydrated, and embedded in Epon. Thin sections were stained with lead citrate-uranyl acetate and examined under a Zeiss 10 electron microscope.

Cell staining and flow cytometry. For flow cytometric measurements, 10^6 PBMC were pelleted, resuspended in 200 μl of PBS, and stained with 2 μl of 100× stock of AO-EB in PBS. The final concentrations of AO (Aldrich, Milwaukee, Wis.) and EB (Sigma) were 0.1 and 0.25 μM, respectively. All samples were stained and analyzed immediately at room temperature.

Flow cytometric analysis was performed on Coulter Profile II (Coulter Corporation, Hialeah, Fla.) and FACScan (Becton Dickinson Immunocytometry Systems, San Jose, Calif.) benchtop cytometers with standard argon ion laser settings (488 nm) and filter sets. Data from the FACScan were acquired and analyzed as presented by using Consort 30 and LYSIS II software, respectively. Cells were sorted using a FACS 440 (Becton Dickinson Immunocytometry Systems) cell sorter equipped with a single argon ion laser and modified with CICERO (Cytomation, Inc., Fort Collins, Colo.) high-speed acquisition and sort electronics. AO and EB were excited at 488 nm and emission detected with a 525/20-nm filter (FL1) and a 635/20-nm filter (FL3), respectively. Four-parameter list mode data were acquired for analysis and sorting. Light scatter parameters were used to gate on single cells, with an acquisition threshold set on the forward scatter (FS) signal. Irradiated cells tended to have more small cell debris that was included above the FSC threshold so as not to include them in the sort window and thus contaminate the sort population. Fluorescence signals were logarithmically amplified, and fluorescence compensation was determined from unlabeled and single-labeled cell controls. Samples were run for several seconds before datum acquisition to allow dye equilibration in the FACS 440 sample tubing. The initial few seconds of sample flow occasionally showed artifacts in staining intensity because of higher background fluorescence from increased sample volume at the interrogation point. Sorting was done with two drop
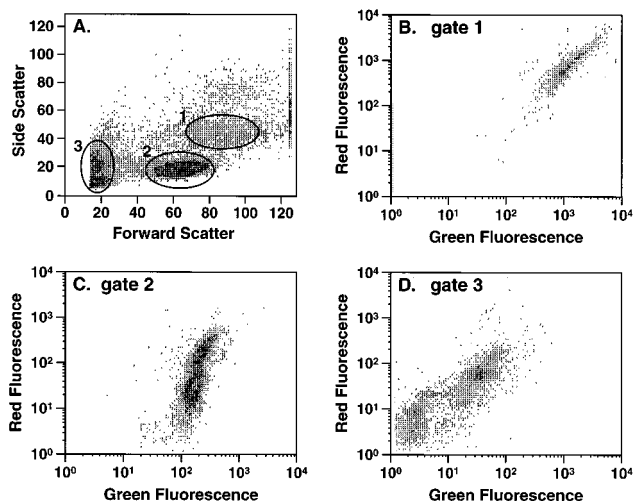

FIG. 1. Bivariate scatter and AO-EB fluorescence dot plots of normal human PBMC. PBMC from healthy donors were isolated and stained with AO and EB. (A) FS (*x* axis) versus SS (*y* axis) light scatter dot plots of ungated cells collected on a linear scale. Distinguishable populations of monocytes versus lymphocytes versus red cells, platelets, and cellular debris are shown as gates 1, 2, and 3, respectively. (B to D) Green (FL1 [*x* axis]) versus red (FL3 [*y* axis]) fluorescence profiles of AO-EB-stained cells from gates 1, 2, and 3, respectively. Fluorescence events were collected on a logarithmic scale.

packets and under conditions to maximize purity over recovery. Nonrectangular sort windows were used on all cell subpopulations of interest. Cells were sorted directly into fixative for EM analysis. Populations were routinely plotted on logarithmic scales as dual-parameter dot plots with AO on the *x* axis (FL1) and EB on the *y* axis (FL3).

Cell populations differentially stained with AO and EB were routinely gated as follows. Population 1 (AO^{high}-EB^{low}) was identified by gating on cells exhibiting high FS. Populations 2 (AO^{low}-EB^{low}) and 3 (AO^{low}-EB^{high}) were identified by gating on cells exhibiting lower FS. Population 2 was defined as all cells with lowered AO staining and EB staining equal to those of population 1. Population 3 was defined as cells showing AO staining lower than and EB staining higher than those of population 1. Cellular debris, erythrocytes, and platelets (very low scatter) were excluded from analysis gates when possible. However, under certain culture conditions, cells showing low FS were continuous with subcellular particles and debris. Most of these events could be differentiated from intact cells when the cells were stained with AO-EB by showing low-fluorescence emission profiles. Infrequently, however, subcellular debris showing relatively high red fluorescence following EB staining could not be removed from the analysis gate and could therefore be included in the AO^{low}-EB^{high} population (see Fig. 5D). In these situations, contaminating debris (showing equal green and red fluorescence) accounted for a small percentage of the cell-associated fluorescence.

RESULTS

Two-dimensional AO-EB staining patterns of untreated and gamma-irradiated PBMC. PBMC are a heterogeneous mixture of leukocytes consisting of lymphocytes (T, B, and NK cells) and monocytes. Lymphocytes, monocytes, and contaminating erythrocytes, platelets, and debris may be differentiated by size, shape, and granularity on the basis of FS and SS properties (45). A scatter plot typical of live, resting PBMC is shown in Fig. 1A, in which circled (gated) populations 1, 2, and 3 correspond to monocytes, to lymphocytes, and to erythrocytes, platelets, and debris, respectively. When PBMC are stained with low concentrations of AO (0.1 μM) and EB (0.25 μM), the green (FL1) versus red (FL3) fluorescence profile reveals three distinct populations, each of which correlates with one of the three gated populations on the basis of scatter profiles. Monocytes (gate 1) exhibit relatively high red and green fluorescence. Lymphocytes (gate 2) exhibit lower green and red fluorescence, such that the green fluorescence falls within a limited range and the red fluorescence exhibits more
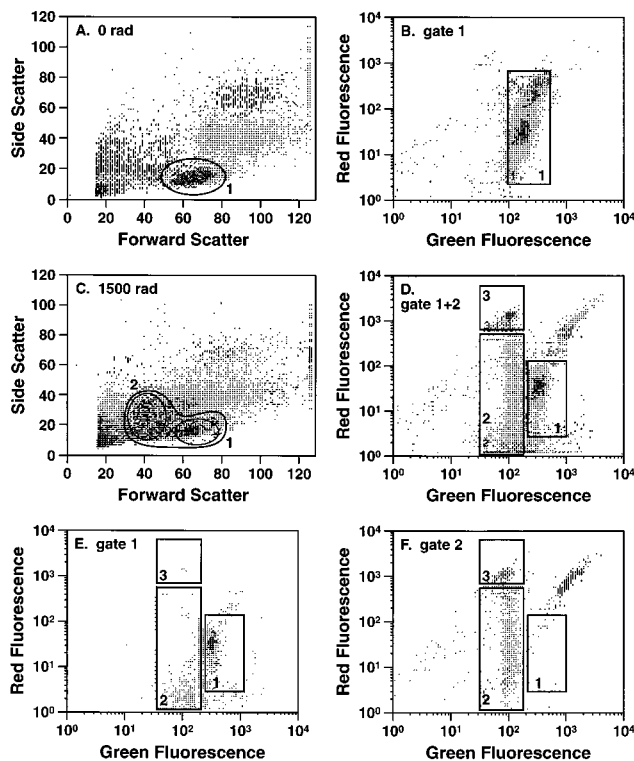
FIG. 2. Irradiation-induced changes in peripheral lymphocyte light scatter and AO-EB fluorescence. Untreated and irradiated (1,000 rads, 10 Gy) PBMC were incubated in complete medium (RPMI, penicillin, streptomycin, 10% fetal bovine serum) for 48 h. Cells were then stained with AO and EB and analyzed for light scatter and fluorescence properties. Fluorescence dot plots represent events within the FS versus SS lymphocyte gates. (A and C) Light scatter plots of FS (x axis) versus SS (y axis); (B through F) green (FL1 [x axis]) versus red (FL3 [y axis]) emission. (A and B) Unirradiated PBMC; (C to F) PBMC exposed to 1,000 rads (10 Gy). Boxes 1, 2, and 3 represent AO^{high}, AO^{low}-EB^{low}, and AO^{low}-EB^{high} populations, respectively. Exposure to irradiation induces an additional population showing a downward shift in FS and a slight upward shift in SS compared with unirradiated control cells. The lymphocytes displaying scatter shifts correspond to cells showing reduced green fluorescence and equal or increased red fluorescence compared with the unshifted population. The distribution of events in boxes 1, 2, and 3 is as follows: panel D, 58, 41, and 6%, respectively; panel E, 98, 2, and 0%, respectively; panel F, 20, 70, and 10%, respectively. Triplicate measurements of a single culture from three donors, whether induced or uninduced to undergo apoptosis, yielded a standard error at less than 5% of the mean.

variability in intensity (Fig. 1C). Platelets, erythrocytes, and debris (gate 3), which have lower FS, show the relatively lowest green and red fluorescence (Fig. 1D).

When PBMC are gamma irradiated and grown in culture for various periods of time, reproducible changes occur in lymphocyte morphology as cells begin to die. These changes are reflected in both light scatter properties and AO-EB fluorescence. Figure 2 shows light scatter (Fig. 2A and C) and AO-EB fluorescence (Fig. 2B, D, E, and F) of unirradiated and irradiated (1,000 rads) PBMC following a 48-h incubation in culture. Irradiated cells show an additional population with lower FS and higher SS (Fig. 2C, gate 2) than those for unirradiated cells. Similar scatter patterns have been observed for rodent thymocytes (16, 35, 40, 41) and transformed cell lines (13) treated with agents that induce apoptosis. In such cases, the lowered SS is attributed to dead or dying cells. These two scatter populations show distinct patterns when analyzed for green (AO) versus red (EB) fluorescence. Figure 2 shows the green versus red fluorescence emission profiles from the

low-FS and high-FS populations. Unirradiated lymphocytes with high FS (Fig. 2A, gate 1) show a single population of fluorescent cells (Fig. 2B, box 1). A similar fluorescence pattern is seen with irradiated cells showing high FS (Fig. 2E). Irradiated cells with decreased FS and increased SS (Fig. 2C, gate 2) show an additional population of cells with lowered green fluorescence, which is split between low (Fig. 2F, box 2) and high (Fig. 2F, box 3) levels of red fluorescence. Three populations are therefore observed with AO-EB fluorescence of irradiated lymphocytes (Fig. 2D, gates 1 and 2): AO^{high} (box 1), AO^{low}-EB^{low} (box 2), and AO^{low}-EB^{high} (box 3). The distinction between populations showing low AO and low (box 2) versus high (box 3) EB fluorescence is often obvious. However, a continuum of EB fluorescence may be seen in some samples in which the upper limits of the EB^{high} and the lower limits of the EB^{low} populations are not clear. In these cases, we based the AO^{low}-EB^{low} and AO^{low}-EB^{high} boundary on that seen with live, EB-impermeable cells.

On the basis of reports using these and other DNA-staining dyes in studies of cell death, it is plausible that these three populations represent live, early-stage apoptotic and late-stage apoptotic and necrotic cells, respectively (21, 22, 35). To test this possibility, we carried out further analysis of fluorescence profiles and cellular morphology to identify the physiological basis for each of the three distinct populations.

AO^{low}-EB^{high}-irradiated lymphocytes represent cells with increased membrane permeability. At low concentrations (<10 μM) and under physiological conditions, monomeric AO exhibits a shift in its emission spectrum from green to red when it is bound to double-stranded versus single-stranded nucleic acids, respectively (14). In addition, AO will emit in the red spectrum when it is incorporated into intracellular lysosomes. In order to test whether the irradiated lymphocyte population demonstrating high red and low green fluorescence under simultaneous AO and EB staining is due to increased EB uptake by cells with permeabilized membranes (late-stage apoptotic or necrotic cells) or is due to red emission by AO, we compared the two-dimensional staining profiles of irradiated lymphocytes in the presence of AO alone or of both AO and EB.

Figure 3 shows the results of an experiment in which PBMC were irradiated at a high dosage (3,000 rads), incubated for 48 h to ensure a substantial amount of cell death, and stained with AO-EB or AO alone. When the cells are stained with AO and EB, the three populations AO^{high} (box 1), AO^{low}-EB^{low} (box 2), and AO^{low}-EB^{high} (box 3) are observed (Fig. 3A). Under such a high dosage and lengthy postirradiation incubation, the predominant cell population is AO^{low}-EB^{high}. When cells are stained with AO alone (Fig. 3B), the population with high red fluorescence disappears and shifts into the AO^{low}-EB^{low} population. This shift indicates that the population showing high red fluorescence is due to increased EB permeability into particular lymphocytes following irradiation and is not due to the red emission of AO when it is bound to single-stranded nucleic acid or uptaken up by lysosomes.

Cell sorting and ultrastructural characterization of populations based on AO-EB staining profiles. In order to characterize whether each distinct population defined by AO-EB fluorescence is live, apoptotic, or necrotic, we sorted the three populations and independently analyzed their morphological features by electron microscopy (Fig. 4). Electron micrographs from untreated or irradiated (1,000 rads, 48 h postirradiation) lymphocytes sorted from the AO^{high}-EB^{low} population appear identical, with ultrastructural features consistent with live, resting peripheral lymphocytes (Fig. 4A and B, respectively). Irradiated cells from the AO^{low}-EB^{low} population, on the other hand, reveal the classic features of apoptotic cells (e.g., con-
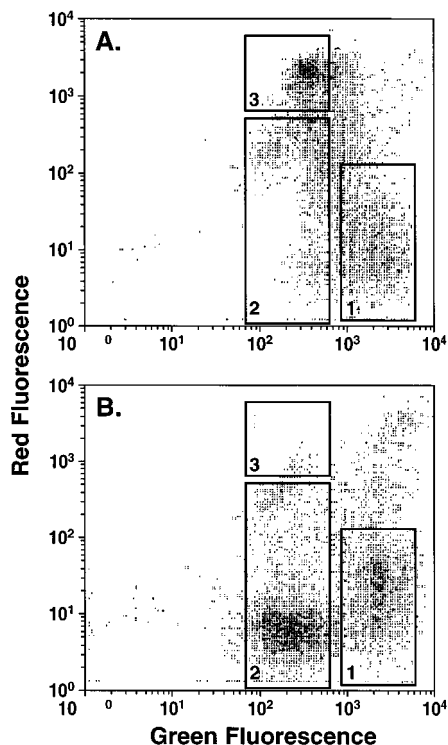
FIG. 3. The increased red fluorescence of irradiated lymphocytes stained with AO-EB is due to increased uptake and fluorescence of EB and not epifluorescence of AO binding to single-stranded nucleic acid. PBMC were irradiated at 3,000 rads (30 Gy), incubated for 48 h at 37°C, and stained with both AO and EB (A) or AO alone (B). Bivariate fluorescence dot plots are shown representing gated lymphocytes based on scatter properties. Three populations are seen when both AO and EB are used (AO^{high}, AO^{low}-EB^{low} and AO^{low}-EB^{high}). Two populations are seen with AO staining alone, AO^{high} and AO^{low}-EB^{low}. In the absence of EB, the AO^{low}-EB^{high} population shifts into the AO^{low}-EB^{low} population, indicating that the high red fluorescence is due to EB and not to AO. The distribution of events in boxes 1, 2, and 3 is as follows: panel A, 31, 27, and 42%, respectively; panel B, 32, 65, and 3%, respectively.

densed nuclei and chromatin, intact cellular membrane and cytoplasmic organelles, and membrane blebbing). The sorted AO^{low}-EB^{high} population represents a predominance of fragmented cells without intact membranes and often damaged intracellular components, making it difficult to unequivocally identify the process of cell death as apoptosis or necrosis. Because some cell remnants appear to have electron dense nuclei, indicating condensed chromatin, it is likely that this population represents a mixture of necrotic and late-stage apoptotic cells in the more advanced stages of deterioration. Compared with unsorted cells, the irradiated and sorted cells are very homogeneous in their appearance. By ultrastructural examination, the frequencies of cells in the sorted populations are as follows ($n = >100$ per sample): $AO^{high} = 97\%$ live and 3% apoptotic; AO^{low}-$EB^{low} = 71\%$ apoptotic and 29% abnormal; and AO^{low}-$EB^{high} = 100\%$ late-stage apoptotic, necrotic, or cellular debris. The predominance of live, apoptotic, and advanced apoptotic and necrotic cells in the AO^{high}, AO^{low}-EB^{low}, and AO^{low}-EB^{high} populations, respectively, supports the interpretation that a downward shift in green fluorescence represents changes in nucleic acid accessibility by AO and/or a reduced overall amount of DNA in cells undergoing apoptosis compared with healthy, live cells. In addition, as cells enter into the later stages of apoptosis (or directly undergo necrosis), the membrane shows increased permeability to vital dyes, as demonstrated here by increased uptake and fluorescence with EB.

Differential AO-EB staining of PBMC and thymocytes after treatment with various apoptosis-inducing agents. Radiation-induced apoptosis in PBMC is a useful but limited model in which to study differential DNA staining during processes of cell death. To test whether differential AO-EB staining of live and apoptotic cells results from cellular changes associated with apoptosis in general or is associated exclusively with radiation-induced DNA damage, we examined the fluorescence of AO-EB-stained human PBMC and mouse thymocytes following exposure to various conditions reported to induce apoptosis. Peripheral lymphocytes show significant apoptosis in culture following exposure to HIV in vivo or in vitro or when activated in vitro with polyclonal mitogens (23, 31, 43). As shown in Fig. 5, these two treatments generate green versus red fluorescence profiles following AO-EB staining that are similar to those seen following irradiation. PBMC from an asymptomatic HIV-seropositive donor show significant cell death by FS and SS (Fig. 5A). In this example, cells were grown in culture in the absence of fetal bovine serum, which further induces apoptosis. Correspondingly, both AO^{high} and AO^{low} populations are present (Fig. 5B). In addition, in vitro activation of PBMC from healthy seronegative donors with the CD4 T-cell-specific superantigen SEB induces blast formation (Fig. 5C) and proliferation but also induces apoptosis in a variable percentage of lymphocytes, as shown by AO^{high} and AO^{low} fluorescence profiles (Fig. 5D). Although the relative positions remain the same, the overall shapes of these cell populations (including very high FS and SS blasts) in scatter and fluorescence profiles vary somewhat with individual donors, indicating heterogeneity in the response to the mitogen.

Murine thymocytes readily undergo apoptosis-associated DNA fragmentation following irradiation or exposure to the corticosteroid dexamethasone (9). Figure 6 shows the light scatter and fluorescence patterns of irradiated or dexamethasone-treated murine thymocytes compared with those exposed to complete culture medium for 24 h. Thymocytes incubated in complete media show both live and dead scatter and AO-EB fluorescence properties (Fig. 6A and B). Treatment with irradiation (Fig. 6C and D), or dexamethasone (Fig. 6E and F) results in virtually all cells showing reduced FS and reduced AO fluorescence. As with HIV-infected PBMC, there appears to be a continuum of low-to-high red fluorescence that display reduced AO fluorescence, suggesting a continuum of membrane permeability to EB following initiation of apoptotic processes. These results indicate that a consistent correlation between scatter and AO-EB fluorescence holds for lymphoid cells regardless of the agent used to induce apoptosis.

Comparison of lymphocyte viabilities by trypan blue uptake and AO-EB staining. Cellular uptake of vital dyes such as trypan blue, which stains only cells with damaged and permeabilized membranes, is an assay that is frequently used to differentiate live from dead cells. However, in the initial stages of apoptosis, the cellular membrane remains intact and perhaps impermeable to such vital dyes (7, 9, 15, 47), potentially yielding an artificially high viability count. To compare postirradiation lymphocyte viabilities using a membrane-exclusive dye alone (trypan blue) versus a combination of membrane-exclusive and nonexclusive dyes (AO-EB), we measured lymphocyte death following irradiation with 300 to 4,500 rads after 24, 48, and 72 h. The results are shown in Fig. 7A to D.

With increased exposure to irradiation dose and length of postirradiation incubation, a decrease in the number of peripheral lymphocytes exhibiting AO^{high} staining is observed (Fig. 7A). Loss of cell viability is both dose and time dependent. A noticeable difference in the numbers of viable cells at each dose occurs between 24 and 48 h; the dose response curves at
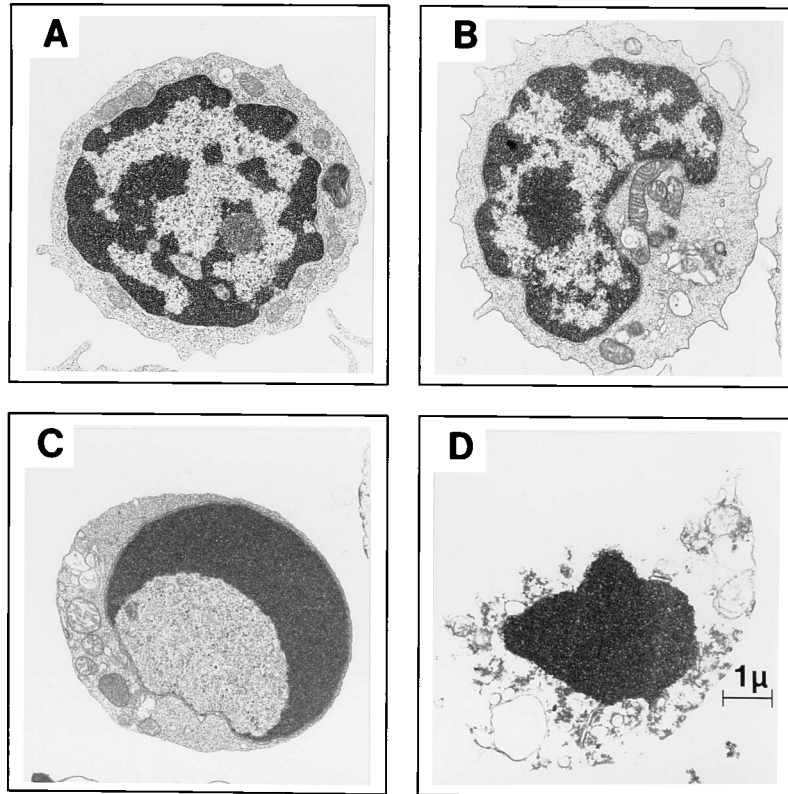
FIG. 4. Cellular sorting and ultrastructural morphology of distinct populations from AO-EB-stained irradiated lymphocytes. PBMC from healthy donors were irradiated with 1,000 rads (10 Gy) and incubated for 48 h. Following staining with AO and EB, cells were sorted into homogeneous populations on the basis of fluorescence properties and were analyzed by electron microscopy. (A) Unirradiated, unsorted lymphocyte; (B) irradiated, sorted lymphocyte from the AO^{high} population (note intact membrane, cellular organelles, and dispersed nuclear heterochromatin); (C) irradiated, sorted lymphocyte from the AO^{low}-EB^{low} population (note intact membrane, cytoplasmic organelles, and condensed nuclear chromatin; (D) irradiated, sorted lymphocyte from the AO^{low}-EB^{high} population (note disintegrated membrane and cellular organelles, condensed nucleus, and electron dense chromatin). The micrographs presented show individual cells representative of each population. PBMC from two donors, cultured independently, were used for each sort. The data represent findings from three independent sets of donors.

48 and 72 h are essentially overlapping. Correspondingly, the numbers of AO^{low}-EB^{low} apoptotic cells (Fig. 7C) and AO^{low}-EB^{high} late-stage apoptotic-necrotic cells (Fig. 7D) increase with radiation dose. Again, irradiation-induced apoptosis is lower at 24 h than at 48 or 72 h.

Cell viability measured by trypan blue also shows a dose and postirradiation time dependency. However, the percentage of live, trypan blue-impermeable cells at a given dose or incubation time is higher than that measured by AO-EB staining (Fig. 7A versus B). In addition, cell death increases in a continuum at 24, 48, and 72 h postirradiation, never reaching the values of cell death as measured by AO-EB staining. These results indicate that AO-EB staining allows increased sensitivity over membrane-impermeable dyes in differentiating live from early-stage apoptotic cells most likely due to AO's uptake by the intact membranes of apoptotic cells.

Fragmentation of chromosomal DNA from irradiated PBMC. Enzymatic digestion of chromosomal DNA into 180- to 200-bp fragments and multimers occurs following induction of apoptosis in many different cell types under different inducing signals (7, 9, 47). Therefore, it was of interest to test whether and to what extent DNA fragmentation occurred in irradiated PBMC. Total cellular DNA was extracted from cells irradiated at various doses and incubated under the conditions described in the legend to Fig. 7. The results are shown in Fig. 8.

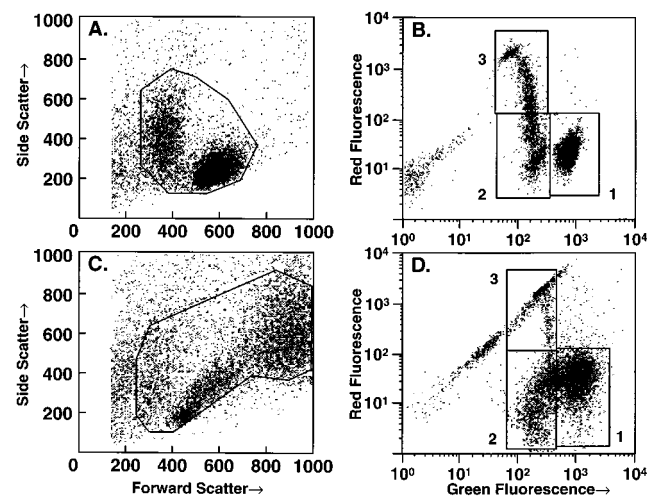In selected samples, 200-kb oligomers of DNA are seen from

FIG. 5. Light scatter and AO-EB fluorescence plots of PBMC undergoing spontaneous and activation-induced apoptosis. (A and B) Light scatter and AO-EB fluorescence dot plots, respectively, of PBMC from an asymptomatic HIV-seropositive subject incubated for 72 h in the absence of 10% fetal bovine serum. The gated events (panels A and C, gate 1) from the scatter plots are shown in the fluorescence dot plots. (C and D) Scatter and fluorescence dot plots of PBMC from a healthy HIV-seronegative donor treated in vitro for 72 h with 1 μg of SEB per ml. In this example, 86% of the cells were viable by trypan blue exclusion. The events in boxes 1, 2, and 3 correspond to AO^{high}-EB^{low}, AO^{low}-EB^{low}, and AO^{low}-EB^{high} populations, respectively. The distribution of events in boxes 1, 2, and 3 is as follows: panel B, 70, 17, and 13%, respectively; panel D, 68, 25, and 7%, respectively.
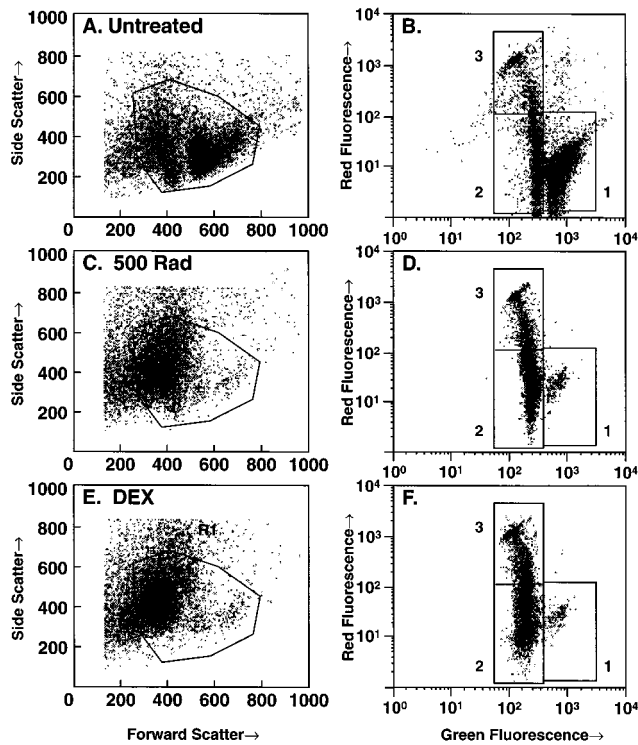
FIG. 6. Light scatter and AO-EB fluorescence profiles of mouse thymocytes undergoing radiation- or corticosteroid-induced apoptosis. Scatter and fluorescence dot plots of mouse thymocytes incubated in complete medium for 24 h following no treatment (A and B) or treatment with 500 rads of gamma irradiation (C and D) or 10^{-7} M dexamethasone (E and F). Fluorescence dot plots consist of the gated events (gate 1) shown in the scatter plots. The distribution of events in boxes 1, 2, and 3 is as follows: panel B, 64, 32, and 4%, respectively; panel D, 4, 77, and 19%, respectively; panel F, 3, 73, and 24%, respectively.
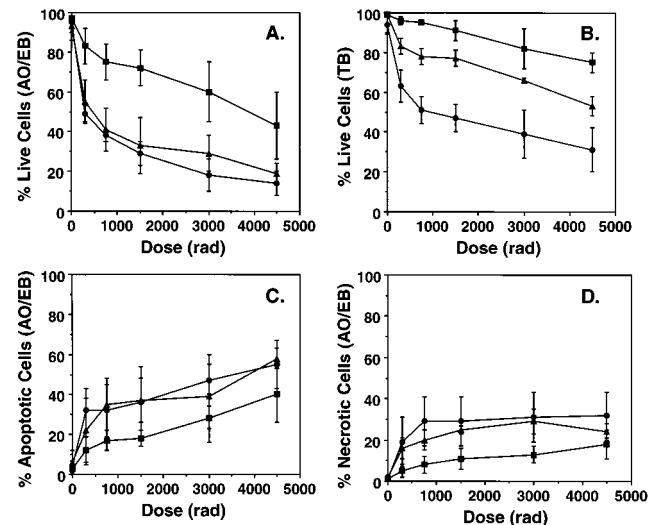

FIG. 7. Comparison of lymphocyte viability by trypan blue uptake and AO-EB staining. PBMC were incubated for 24 (squares), 48 (triangles), or 72 (circles) h at 37°C following 0 to 4,500 rads (0 to 45 Gy) of gamma irradiation. At the various time points, 10^6 cells were pelleted and viability was measured by (i) visualization of trypan blue-excluding cells by light microscopy relative to the total number of trypan blue-excluding and -permeable cells and (ii) AO-EB staining and flow cytometry such that the percentages of live, apoptotic, and late-stage apoptotic and necrotic cells were determined by quantifying the numbers of events in the three distinct AO-EB-staining populations. The x axes represent radiation dosages in rads. The y axes represent the percentages of live cells by AO-EB staining (A) and trypan blue exclusion (B), the percentage of apoptotic cells by AO-EB staining (C), and the percentages of dead cells by AO-EB staining (D). Each point represents the average of four independent experiments using four different donors. Error bars are standard deviations from the average values.

DISCUSSION

We have characterized a method to rapidly quantify mature peripheral lymphocytes undergoing apoptosis on an individual cell basis using a single-laser flow cytometer with standard laser settings and filters. The method is based on differential uptake and DNA staining of AO and EB, which, when used

samples incubated for 24, 48, and 72 h postirradiation. No significant DNA fragmentation is observed in samples of unirradiated control lymphocytes. Of the samples that did show fragmentation, a substantial amount of high-molecular-weight DNA is present, suggesting that either a small subset of cells have undergone internucleosomal DNA digestion and/or that only a fraction of each cell's DNA ultimately becomes fragmented. The most extensive fragmentation is seen following exposure to 300 to 1,500 rads and 24-, 48-, or 72-h incubations. Similar fragmentation patterns have been observed for lymphocytes incubated for up to 6 days postirradiation at 1,500 rads (data not shown). If DNA fragmentation is an early event in apoptosis, as seen in rodent thymocytes (8), our results suggest that fragmented intracellular DNA is relatively stable and/or that cells are continuously undergoing apoptosis up to 72 h postirradiation. Interestingly, at higher doses (3,000 or 4,500 rads), fragmented DNA is barely detectable or nonexistent at any time postirradiation. As observed by others, high radiation dosage may elicit cell death that cannot be characterized by the classic markers of apoptosis or necrosis (36). Although cell viability decreases with increased radiation dose and length of postirradiation incubation, no such correlation is evident in the presence of DNA fragmentation. This underscores the independence of DNA fragmentation from other morphological markers of apoptosis (6, 10).
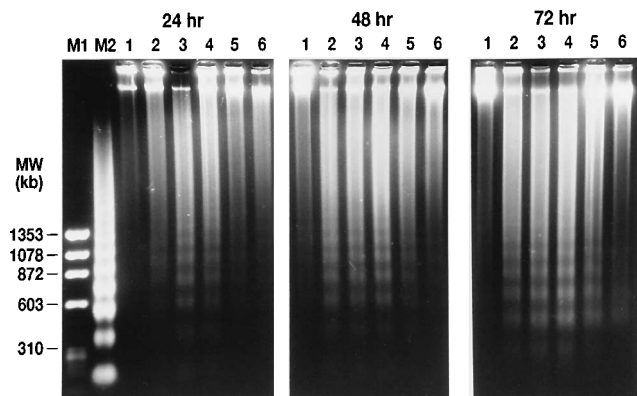

FIG. 8. Fragmentation of chromosomal DNA from irradiated PBMC. PBMC were irradiated with 0 to 4,500 rads (0 to 45 Gy) and were incubated in culture for 24, 48, or 72 h. Whole cellular DNA was extracted from 2×10^6 cells and was fractionated by agarose gel electrophoresis, stained with EB, and visualized with UV (254-nm-wavelength) light. M1 and M2 represent molecular-weight standards consisting of φX174/HaeIII-digested DNA and DNA from mouse thymocytes which have undergone irradiation-induced (500 rads) apoptosis, respectively. Lanes represent dosages as follows: 1, 0 rads; 2, 300 rads; 3, 750 rads; 4, 1,500 rads; 5, 3,000 rads; and 6, 4,500 rads.

together in low concentrations at equilibrium, create three distinct lymphocyte populations that stain (i) brightly for AO but that are impermeable to EB (AO^{high}-EB^{low}), (ii) dimly for AO and that are impermeable to EB (AO^{low}-EB^{low}), and (iii) dimly for AO and that are permeable to EB (AO^{low}-EB^{high}). We have identified the cells in these populations as live, apoptotic, and late-stage apoptotic and necrotic, respectively, by cell sorting and ultrastructural examination of electron micrographs. The relative numbers of cells in each population can be determined by electronic gating, allowing accurate quantification of cells in each stage.

Recently, other reports have described methods which differentiate live and apoptotic cells using a single nucleic acid-binding dye with fixed or detergent-permeabilized cells (29, 33, 41, 42, 49) in which apoptotic cells show decreased staining. However, fixation and permeabilization methods can yield inconsistent light scatter and fluorescence characteristics. An important advantage in using a combination of two nucleic acid-binding dyes (one that enters live cells with intact membranes and one that does not) is that it allows differentiation of the early and late stages of apoptosis on the basis of their differential membrane characteristics. Studies using single dyes with fixed cells lose this distinction, with all dimly stained cells grouped into one population. Similarly, methods which rely on scoring cell death using unfixed cells and vital dyes such as trypan blue will miss apoptotic cells in the early stages, when membranes are still intact. This is illustrated in Fig. 7, in which the number of dead or dying lymphocytes measured by trypan blue at a particular radiation dose or incubation time is consistently lower than that measured by AO-EB staining.

Multiparameter analysis of cells stained with Hoechst dyes is reported to differentiate live from apoptotic cells (15, 16, 24, 28, 34, 35, 37, 38, 40). The increased blue fluorescence of apoptotic thymocytes has been attributed to increased uptake of the Hoechst dye (35). However, in at least one report, the apoptotic population is shown to exhibit decreased fluorescence (5). This discrepancy may reflect factors involved in cell fluorescence by Hoechst dyes, including dye uptake, binding, and efflux that may be differentially affected in different cell types or with different apoptosis-inducing agents (35), possibly posing a disadvantage over AO-EB staining. In addition, the Hoechst dyes, in combination with EB or propidium iodide, require additional lasers compared with those needed for AO-EB analysis.

It is not clear what mechanism or combination of mechanisms accounts for the observed downward shift in AO staining seen with apoptotic cells. It has been argued that the reduced fluorescence of nucleic acid-binding dyes such as AO is due to reduced accessibility because of changes in chromatin conformation and protein content during apoptosis (42) or DNA loss following digestion and extrusion by apoptotic bodies (13, 35). Although our studies do not directly address this issue, we do show distinct downward shifts in AO staining without oligomeric DNA fragmentation (and presumably subsequent loss) in samples in which PBMC were irradiated with higher doses (3,000 or 4,500 rads). In addition, all fluorescence measurements were made on cells in the absence of agents that permeabilize membranes, reducing the opportunity for significant DNA loss. It is possible that abundant DNA loss is a distinct factor in cells such as mouse thymocytes, in which DNA fragmentation following induction of apoptosis is extensive. However, in apoptotic human peripheral lymphocytes, DNA fragmentation and ultimate loss appears much less extensive and thus is an unlikely sole explanation for the observed reduction in AO binding and fluorescence.

There are many advantages to using flow cytometry in scor-

ing apoptotic cells. When a heterogeneous population is analyzed with respect to lineage or developmental stage, distinct cell subsets can be differentiated by electronic gating on the basis of light scatter properties. When used in combination with light scatter, fluorescence analysis of distinct populations in a single sample increases the power of analysis by delineating subsets defined by classic light scatter properties. Additionally, apoptosis is measured on an individual cell basis without the elements of intra- and interobserver subjectivity inherent in microscope-based assays. More importantly, the data are not averaged over a particular sample that may be a mixture of live, apoptotic, and necrotic cells.

We find that this flow cytometric method is significantly more accurate and reproducible than quantifying apoptosis by DNA fragmentation, in which relative amounts of lower- versus high-molecular-weight DNA are taken as measures of the relative numbers of apoptotic versus live cells, respectively (3, 32, 43). Because such measurements can be considered accurate only if complete digestion without significant DNA loss can be assumed, they are not suitable for many cell types, including PBMC, in which DNA fragmentation is incomplete, as demonstrated here. Recent reports (19, 20) describing quantitative measurement of DNA breakage in individual cells can overcome this problem, but only in systems in which fragmentation clearly correlates with other apoptotic markers. In this report, DNA fragmentation did not always correlate with apoptosis, as measured by three independent methods: AO-EB staining, electron microscopy, and vital dye exclusion. High-irradiation doses showed significant cell death in the absence of DNA fragmentation. These findings are consistent with other reports showing a lack of correlation between DNA fragmentation and other apoptotic markers (6, 10) and underscore the need to measure multiple markers of cell viability for unequivocal differentiation.

The changes in fluorescence patterns described here that correlate with radiation-induced apoptosis are also observed with peripheral lymphocytes and thymocytes undergoing apoptosis initiated by inducers that are more physiological than gamma irradiation. Flow cytometric analysis of AO-EB-stained lymphoid cells offers a novel approach by which to study agents suspected to induce inappropriate apoptosis in vivo, leading to a wide variety of disease states (11, 12, 25, 46). For example, we and others (21, 22) have measured lowered AO staining in in vitro cultures of PBMC from HIV-infected individuals that correlates with apoptotic cell death as measured by independent assays (23, 31). Thus, flow cytometric analysis of AO-EB-stained cells has broad applicability to detecting and quantifying apoptotic cells of lymphoid and perhaps other tissue origins induced by a variety of agents.

REFERENCES

1. **Akbar, A. N., N. Borthwick, M. Salmon, W. Gombert, M. Bofill, N. Shamsadeen, D. Pilling, S. Pett, J. E. Grundy, and G. Janossy.** 1993. The significance of low bcl-2 expression by CD45RO T cells in normal individuals and patients with acite viral infections. The role of apoptosis in T cell memory. J. Exp. Med. **178:**427–438.
2. **Arends, M. J., R. G. Morris, and A. H. Wyllie.** 1990. Apoptosis: the role of the endonuclease. Am. J. Pathol. **136:**593–608.
3. **Banda, N. K., J. Bernier, D. K. Kurahara, R. Kurrle, N. Haigwood, R.-P.**

Sekaly, and T. H. Finkel. 1992. Crosslinking CD4 by human immunodeficiency virus gp120 primes T cells for activation-induced apoptosis. J. Exp. Med. **176:**1099–1106.

4. **Carson, D. A., and J. M. Ribeiro.** 1993. Apoptosis and disease. Lancet **341:**1251–1254.

5. **Chrest, F. J., M. A. Buchholz, Y. H. Kim, T.-K. Kwon, and A. A. Nordin.** 1993. Identification and quantitation of apoptotic cells following anti-CD3 activation of murine G_o T cells. Cytometry **14:**883–890.

6. **Cohen, G. M., X.-M. Sun, R. T. Snowden, D. Dinsdale, and D. N. Skilleter.** 1992. Key morphological features of apoptosis may occur in the absence of internucleosomal fragmentation. Biochem. J. **286:**331–334.

7. **Cohen, J. J.** 1991. Programmed cell death in the immune system. Adv. Immunol. **50:**55–85.

8. **Cohen, J. J., and R. C. Duke.** 1984. Glucocorticoid activation of a calcium-dependent endonuclease in thymocyte nuclei leads to cell death. J. Immunol. **132:**38–42.

9. **Cohen, J. J., R. C. Duke, V. A. Fadok, and K. Sellins.** 1992. Apoptosis and programmed cell death in immunity. Annu. Rev. Immunol. **10:**276–293.

10. **Collins, R. J., B. V. Harmon, B. C. Gobe, and J. F. Kerr.** 1992. Internucleosomal DNA cleavage should not be the sole criterion for identifying apoptosis. J. Radiat. Biol. **61:**451–453.

11. **Compton, M. M., J. S. Haskill, and J. A. Cidlowski.** 1988. Analysis of glucocorticoid actions on rat thymocyte deoxyribonucleic acid by fluorescence-activated flow cytometry. Endocrinology **122:**2158–2164.

12. **Dancescu, M., M. Rubio-Trujillo, G. Biron, D. Bron, G. Delespesse, and M. Sarfate.** 1992. Interleukin 4 protects chronic lymphocytic leukemic B cells from death by apoptosis and upregulates Bcl-2 expression. J. Exp. Med. **176:**1319–1326.

13. **Darzynkiewicz, Z., S. Bruno, G. Del Bino, W. Gorczyca, M. A. Hotz, P. Lassota, and F. Traganos.** 1992. Features of apoptotic cells measured by flow cytometry. Cytometry **13:**795–808.

14. **Darzynkiewicz, Z., and J. Kapuscinski.** 1990. Acridine orange: a versatile probe of nucleic acids and other cell constituents, p. 291–314. *In* M. R. Melamed, T. Lindmo, and M. L. Mendelsohn (ed.), Flow cytometry and sorting, 2nd ed. J. Wiley & Sons, Inc., New York.

15. **Del Bino, G., P. Lassota, and Z. Darzynkiewicz.** 1991. The S-phase cytotoxicity of captothecin. Exp. Cell Res. **193:**27–35.

16. **Dive, C., C. D. Gregory, D. J. Phipps, D. L. Evans, A. E. Milner, and A. H. Wyllie.** 1992. Analysis and discrimination of necrosis and apoptosis (programmed cell death) by multiparameter flow cytometry. Biochem. Biophys. Acta **1133:**275–285.

17. **Duke, R. C., R. Chervenak, and J. J. Cohen.** 1983. Endogenous endonuclease-induced DNA fragmentation: an early event in cell mediated cytolysis. Proc. Natl. Acad. Sci. USA **80:**6361–6365.

18. **Evan, G. I., A. H. Wyllie, C. S. Gilbert, T. D. Littlewood, H. Land, M. Brooks, C. M. Waters, L. Z. Penn, and D. C. Hancock.** 1992. Induction of apoptosis in fibroblasts by c-*myc* protein. Cell **69:**119–128.

19. **Gorczyca, W., S. Bruno, R. J. Darzynkiewicz, J. Gong, and Z. Darzynkiewicz.** 1992. DNA strand breaks occurring during apoptosis: their in situ detection by the terminal deoxynucleotidyl transferase and nick translation assays and prevention by serine protease inhibitors. Int. J. Oncol. **1:**639–648.

20. **Gorczyca, W., J. Gong, and Z. Darzynkiewicz.** 1993. Detection of DNA strand breaks in individual apoptotic cells by the in situ terminal deoxytransferase and nick translation assays. Cancer Res. **53:**1945–1951.

21. **Gougeon, M.-L., S. Garcia, D. Guetard, R. Olivier, C. Dauguet, and L. Montagnier.** 1992. Apoptosis as a mechanism of cell death in peripheral lymphocytes from HIV-1 infected individuals. Immunodeficiency in HIV infection and AIDS, p. 115–126. *In* G. Janossy, B. Autran, and F. Miedema (ed.), EC/FERS/MRC workshop on immunodeficiency in HIV-1 infections. Karger, Basel.

22. **Gougeon, M.-L., R. Oliver, S. Garcia, D. Guetard, T. Dragic, C. Dauget, and L. Montagnier.** 1991. Demonstration of a process leading to cellular death by apoptosis in lymphocytes from HIV infected patients. C.R. Acad. Sci. Paris **312:**529–537.

23. **Groux, H., G. Torpier, D. Monte, Y. Mouton, A. Capron, and J. C. Amiesen.** 1992. Activation-induced death by apoptosis in CD4+ T cells from human immunodeficiency virus-infected asymptomatic individuals. J. Exp. Med. **175:**331–340.

24. **Hardin, J. A., D. H. Sherr, M. A. DeMaria, and P. Lopez.** 1992. A simple fluorescence method for surface antigen phenotyping of lymphocytes undergoing DNA fragmentation. J. Immunol. Methods **154:**99–107.

25. **Henderson, S., M. Bowe, C. Gregory, D. Croom-Carter, F. Wang, R. Longnecker, E. Kieff, and A. Rickinson.** 1991. Induction of *bcl*-2 expression by Epstein-Barr virus latent membrane protein 1 protects infected B cells from programmed cell death. Cell **65:**1107–1115.

26. **Hockenberry, D., G. Nunez, L. Milliman, R. D. Schreiber, and S. J. Korsmeyer.** 1990. *bcl*-2 is an inner mitochondrial membrane protein that blocks programmed cell death. Nature (London) **248:**334–336.

27. **Hotz, M. A., J. Gong, F. Traganos, and Z. Darzynkiewicz.** 1994. Flow cytometric detection of apoptosis: comparison of the assays of in situ DNA degradation and chromatin changes. Cytometry **15:**237–244.

28. **Kerr, J. F. R., A. H. Wyllie, and A. R. Currie.** 1972. Apoptosis: a basic biological phenomenon with wide-ranging implication in tissue kinetics. Br. J. Cancer **26:**239–257.

29. **Kubbies, M.** 1990. Flow cytometric recognition of clastogen induced chromatin damage in G0/G1 lymphocytes by non-stoichiometric Hoechst fluorochrome binding. Cytometry **11:**386–394.

30. **Lyons, A. B., K. Samuel, A. Sanderson, and A. H. Maddy.** 1992. Simultaneous analysis of immunophenotype and apoptosis of murine thymocytes by single laser flow cytometry. Cytometry **13:**809–820.

31. **Meyaard, L., S. A. Otto, R. R. Jonker, M. J. Mijnster, R. P. Keet, and F. Miedema.** 1992. Programmed death of T cells in HIV-1 infection. Science **257:**217–219.

32. **Newell, M. K., L. J. Haughn, C. R. Maroun, and M. H. Julius.** 1990. Death of mature T cells by separate ligation of CD4 and the T-cell receptor for antigen. Nature (London) **347:**286–288.

33. **Nicoletti, I., G. Migliorati, M. C. Pagliacci, F. Grignani, and C. Riccardi.** 1991. A rapid and simple method for measuring thymocyte apoptosis by propidium iodide staining and flow cytometry. J. Immunol. Methods **139:**271–279.

34. **Ormerod, M. G., M. K. Collins, L. G. Rodriguez-Tarduchy, and D. Robertson.** 1992. Apoptosis in interleukin-3-dependent haemopoietic cells. Quantification by two cytometric methods. J. Immunol. Methods **153:**57–65.

35. **Ormerod, M. G., X.-M. Sun, R. T. Snowden, R. Davies, H. Fearnhead, and G. M. Cohen.** 1993. Increased membrane permeability of apoptotic thymocytes: a flow cytometric study. Cytometry **14:**595–602.

36. **Payne, C. M., C. G. Bjore, and D. A. Schultz.** 1992. Change in the frequency of apoptosis after low- and high-dose X-irradiation of human lymphocytes. J. Leukocyte Biol. **52:**433–440.

37. **Schmid, I., C. H. Uittenbogaart, J. V. Giorgi.** 1994. Sensitive method for measuring apoptosis and cell surface phenotype in human thymocytes by flow cytometry. Cytometry **15:**12–20.

38. **Schmid, I., C. H. Uittenbogaart, B. Keld, and J. V. Giorgi.** 1994. A rapid method for measuring apoptosis and dual-color immunofluorescence by single laser flow cytometry. J. Immunol. Methods **170:**145–157.

39. **Sellins, K. S., and J. J. Cohen.** 1987. Gene induction by γ-irradiation leads to DNA fragmentation in lymphocytes. J. Immunol. **139:**3199–3206.

40. **Sun, X.-M., R. T. Snowdon, D. N. Skilleter, and D. Dinsdale.** 1992. A flow-cytometric method for the separation and quantitation of normal and apoptotic thymocytes. Anal. Biochem. **204:**351–356.

41. **Swat, W., L. Ignatowicz, and P. Kisielow.** 1991. Detection of apoptosis of immature $CD4^+8^+$ thymocytes by flow cytometry. J. Immunol. Methods **137:**79–87.

42. **Telford, W. G., L. E. King, and P. J. Fraker.** 1992. Comparative evaluation of several DNA binding dye in the detection of apoptosis-associated chromatin degradation by flow cytometry. Cytometry **13:**137–143.

43. **Terai, C., R. S. Kornbluth, C. D. Pauza, D. D. Richman, and D. A. Carson.** 1991. Apoptosis as a mechanism of cell death in cultured T lymphoblasts acutely infected with HIV-1. J. Clin. Invest. **87:**1710–1715.

44. **Vaux, D. L., S. Cory, and J. M. Adams.** 1988. *bcl*-2 gene promotes haemopoietic cell survival and cooperates with c-*myc* to immortalize pre-B cells. Nature (London) **335:**440–442.

45. **Visser, J. W. M., G. J. van den Engh, and D. W. van Bekkum.** 1980. Light scattering properties of murine hemopoietic cells. Blood Cells **6:**391–407.

46. **Watanabe-Fukunaga, R., C. I. Brannan, N. G. Copeland, N. A. Jenkins, and S. Nagata.** 1992. Lymphoproliferation disorder in mice explained by defects in FAS antigen that mediates apoptosis. Nature (London) **356:**314–317.

47. **Wyllie, A. H., J. F. R. Kerr, and A. R. Currie.** 1980. Cell death: the significance of apoptosis. Int. Rev. Cytol. **68:**251–306.

48. **Wyllie, A. H., K. A. Rose, R. G. Morris, E. Steel, E. Foster, and D. A. Spandidos.** 1987. Rodent fibroblast tumours expressing human *myc* and *ras* genes: growth, metastasis, and endogenous oncogene expression. Br. J. Cancer **56:**251–259.

49. **Zamai, L., G. Falceri, A. Cataldi, and M. Vitale.** 1993. Optimal detection of apoptosis by flow cytometry depends on cell morphology. Cytometry **14:**891–897.